RSC Advances

PAPER

View Article Online
View Journal | View Issue

Cite this: *RSC Adv.*, 2025, **15**, 13119

In situ thermal-responsive hydrogels for combined photothermal therapy and chemotherapy of pancreatic cancer †

Ningwei Wang,[a] Xu Yan,[b] Chaofei Ji,[c] Jinlong Hu,[d] Xiangshun Chen,[b] Cong Zhang,[a] Yuzhu Quan,[e] Tao He, *[b] Tianci Sun*[b] and Yue Yu *[a]

Received 15th January 2025
Accepted 14th February 2025

DOI: 10.1039/d5ra00371g

rsc.li/rsc-advances

Pancreatic cancer is a malignancy with a poor prognosis and high mortality. Survival outcomes remain very poor despite significant advances in molecular diagnostics and therapeutics in clinical practice. Surgical resection is the only potentially curative treatment, but the tumor is often diagnosed at an advanced stage, and most cancers recur after surgery. Treatments other than surgery, including chemotherapy and immunotherapy, still offer disappointing results. Multidisciplinary treatment approaches through appropriate carriers have provided new solutions for improving the prognosis of pancreatic cancer. Herein, we reported an *in situ* formed thermo-responsive hybrid hydrogel loaded with gemcitabine and manganese dioxide nanoparticles, which exhibited good injectability, high photothermal hyperthermia, and biocompatibility, leading to efficient multidisciplinary treatment of pancreatic cancer in combination with chemotherapy and photothermal therapy (PTT). The hybrid hydrogel could be heated to 51 °C under 808 nm laser irradiation in five minutes. *In situ* intratumoral injection results suggested that the hybrid hydrogel exhibited high photothermal efficiency in killing rabbit pancreatic tumors. *In vivo* results indicated that the multidisciplinary treatment almost completely eliminated subcutaneous tumors in mice within 14 days. This development offers an efficient multidisciplinary treatment for pancreatic cancer.

Introduction

Pancreatic cancer (PC) mainly refers to malignant tumors of the pancreatic exocrine glands, with ductal adenocarcinoma being the most predominant pathological type of pancreatic cancer. As one of the most malignant tumors, with the shortest survival period and the highest mortality rate,[1,2] pancreatic cancer lacks effective early screening methods and has a limited number of treatment options, earning it the title of the "king of cancers".[3] The incidence of pancreatic cancer is increasing, with an annual growth rate of 0.5–1.0%, and it is expected to become the second most prominent contributor to cancer-related mortality by the year 2030.[4] Only limited treatment options have been approved for PC, including surgical resection, chemotherapy, immunotherapy, and targeted therapies. Although the survival time of PC patients can be improved by complete surgical resection, PC is usually diagnosed at advanced stages, with most patients presenting with locally advanced (30–35%) or metastatic (50–55%) pancreatic cancer at the time of diagnosis, forfeiting the opportunity for surgery.[5] Less than 20% of patients are eligible for potentially curative surgery.[6] Chemotherapy remains the cornerstone of treatment for PC. For patients with resectable or borderline resectable PC, adjuvant chemotherapy is employed after surgical resection. Owing to the unique pathobiological features of PC—a nearly impenetrable desmoplastic stroma and hypovascular, hypoperfused tumor vessels—most treatment options other than surgical resection are largely ineffective.[7] Due to insufficient perfusion and vascularity, the tumor microenvironment in PC is generally hypoxic, which diminishes the effectiveness of photodynamic and photothermal therapies.[7,8] Hypoxia results in the activation of pancreatic stellate cells within the tumor stroma by inflammatory cytokines, leading to the development of fibrosis and cancer cell invasion.[9–11] Further, hypoxia promotes tumor progression, invasion, metastasis, and drug resistance.[12] Even though comprehensive regimens of multiple treatments for

[a]*Department of Gastroenterology, Centre for Leading Medicine and Advanced Technologies of IHM, The First Affiliated Hospital of USTC, Division of Life Sciences and Medicine, University of Science and Technology of China, Hefei, 230001, China. E-mail: yuyuemd@ustc.edu.cn*

[b]*Anhui Province Key Laboratory of Value-Added Catalytic Conversion and Reaction Engineering, Anhui Province Engineering Research Center of Flexible and Intelligent Materials, School of Chemistry and Chemical Engineering, Hefei University of Technology, Hefei, 230001, China. E-mail: taohe@hfut.edu.cn; suntianci@mail.hfut.edu.cn*

[c]*Department of Radiology, Anhui No. 2 Provincial People's Hospital, Hefei, 230001, China*

[d]*Department of General Surgery, Anhui No. 2 Provincial People's Hospital, Hefei, 230001, China*

[e]*Changchun GeneScience Pharmaceutical Co., Ltd., Xuhui District, Shanghai, 200030, China*

† Electronic supplementary information (ESI) available. See DOI: https://doi.org/10.1039/d5ra00371g

patients have been developed, the current 5 year survival rate for all stages remains as low as 9%.[13]

Gemcitabine (GEM) is a pyrimidine antimetabolite that inhibits DNA synthesis and has been recognized as the cornerstone of PC cytotoxic therapy in all stages of the disease, despite suboptimal clinical outcomes primarily caused by molecular mechanisms limiting its cellular uptake. This often results in chemoresistance within weeks of treatment initiation.[14–18] To circumvent GEM resistance in PC, new therapeutic approaches have been developed, including chemical modification of the GEM molecule and alteration of the drug delivery pathway. Meanwhile, many new prodrugs, such as nanoparticles and liposomes, have been investigated and developed.[19,20] However, although animal experiments have shown improvements in the therapeutic efficacy of these new products in cellular experiments and small animal tumor model systems, translational clinical applications are still in the very early stages, and systemic side effects remain an unavoidable challenge.[21]

Several factors contribute to the poor efficiency of current treatments. For example, the dense stromal tissue of PC acts like an iron wall, preventing the penetration of drugs from the systemic circulation. Additionally, PC is lacks a vascular tumor network. The deficiency of microvasculature further decreases the exchange of substances between the tumor and the systemic circulation, resulting in extremely low drug uptake efficiency and higher drug side effects.[7,22,23] Most drug modifications and targeted therapies pale in the face of the specific tumor-suppressive microenvironment and histological features of pancreatic cancer, while traditional intravenous drug delivery and immunotherapy are ineffective for PC. There is a constant impetus to develop novel treatments with higher efficiency.

Recently, as a platform for local combination therapy, hydrogels have emerged as a hotspot for biomedical and pharmaceutical applications due to their biocompatibility, adjustable physicochemical properties, controllable structure and feasibility for multiple functionalizations.[24,25] Various functional hydrogels have been reported for use in encapsulating therapeutic cells,[24] drugs,[26–28] nanoparticles,[29] and immune factors.[30] Promising therapeutic prospects in clinical applications have been demonstrated. For example, Yan *et al.*[31] prepared thermosensitive hydrogel with iron oxide nanoparticles to form a magnetic hydrogel, which was able to perform hemostasis, magnetic hyperthermia and transarterial embolization, improving the treatment effect for liver cancer. Ning *et al.*[32] amalgamated hexadecylamine and nanocellulose to construct a hydrogel network that prolonged the release period of loaded paclitaxel (PTX), amplifying its anticancer efficacy. Subsequent *in vitro* cytotoxicity investigations on HepG2 and A549 cells further underscored the cellulose-based hydrogel composite's potential in combating cancer. However, to our knowledge, there are no reports applying hydrogels for minimally invasive local therapy in the treatment of unresectable PC, which is clearly an area worth exploring, given the potential to address the disadvantages of present therapies, along with the benefits that local therapy may bring.

Herein, we demonstrated the preparation of a thermo-responsive hybrid hydrogel and its application to achieve synergistic ablation and local chemotherapy treatment of PC. PEG-modified manganese dioxide nanoparticles (denoted as MnO_2–PEG NPs) and GEM were incorporated into the pre-synthesized poly((*N*-isopropylacrylamide-*co*-dopamine)-*b*-poly(-ethylene glycol)-*b*-poly(*N*-isopropylacrylamide-*co*-dopamine)) (poly(NIPAM-*co*-DOPA)–PEG–poly(NIPAM-*co*-DOPA)) (denoted as DTBP) matrix to produce the thermo-responsive hydrogel (Scheme 1). This hydrogel exhibited good injectability through different types of needles, which encouraged invasive administration. The hybrid hydrogel could be heated to 51 °C in 5 minutes under 808 nm laser irradiation, and through the combination of chemotherapy and photothermal therapy, subcutaneous tumors in mice were almost completely eliminated within 14 days. This treatment platform was demonstrated to be a safe and well-tolerated intervention for PC by evaluating the foreign body response and biocompatibility of the injectable composite hydrogel. This local therapy will impact the development of various efficient PC treatments. We envisage that multidisciplinary approaches to cure unresectable PC will be established based on the efficacy of the composite hydrogel.

Experimental section/methods

Materials

All chemicals were purchased from Aldrich and used as received unless otherwise stated. *N*-Isopropylacrylamide (NIPAM) was purified by recrystallisation from *n*-hexane.

Preparation of DTBP

Synthesis of tri-block copolymers of poly((*N*-isopropylacrylamide$_{63}$-*co*-dopamine$_{17}$)-*b*-poly(ethylene glycol)-*b*-

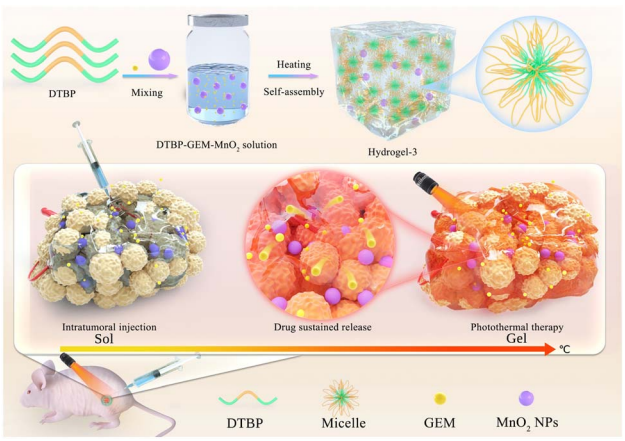

Scheme 1 Schematic of hydrogel treatment for pancreatic cancer. The pre-gel aqueous suspensions quickly transformed into a solid gel when triggered by temperature (28 °C). The hydrogel suspension was injected into the pancreatic cancer tumor, followed by a combination of photothermal and chemotherapy treatment. Under 808 nm laser irradiation, the hydrogel simultaneously heated and released the drug.

poly(*N*-isopropylacrylamide$_{63}$-*co*-dopamine$_{17}$)) (poly(NIPAM$_{63}$-*co*-DOPA$_{17}$)–p(ethylene glycol)$_{90}$–poly(NIPAM$_{63}$-*co*-DOPA$_{17}$)).

Macro-CTA was synthesized according to a previous report. Typically, polyoxyethylene bis(amine) (M_w = 4 kDa) (0.40 g, 0.1 mmol), 4-cyano-4-(phenylcarbonothioylthio)pentanoic acid *N*-succinimidyl ester (0.15 g, 0.4 mmol) and trimethylamine (0.06 g, 0.6 mmol) were dissolved in 20 mL dichloromethane. After flushing with N_2 for 10 min, the mixture was stirred at room temperature for 10 h. Dichloromethane was removed under vacuum, and the mixture was precipitated in ethyl ether (30 mL), followed by drying under vacuum. Macro-CTA was obtained as a pink solid. The reversible addition–fragmentation chain transfer (RAFT) polymerization of NIPAM (0.996 g) and *N*-succinimidyl acrylate (NSA) (0.186 g) was conducted to produce the block polymer poly((*N*-isopropylacrylamide-*co*-*N*-succinimidyl-acrylate)-*b*-poly(ethylene glycol)-*b*-poly(*N*-isopropylacrylamide-*co*-*N*-succinimidyl acrylate)) (poly(NIPAM-*co*-NSA)–PEG–poly(NIPAM-*co*-NSA)) in the presence of macro-CTA. In the next step, dopamine functional groups were conjugated onto the polymer chains *via* an amination reaction, yielding the final polymer, DTBP. GPC curves (solvent: tetrahydrofuran) of TBP showed M_w = 24.0 kDa, $Đ$ = 1.69.

Preparation of MnO_2–PEG NPs

50 mg of commercially available MnO_2 NPs was dissolved in 10 mL of deionized water, sonicated for 5 min, and then 1 g of OH–PEG (M_w = 5 kD) was added and stirred at 500 rpm for 60 min at room temperature. Dialysis was performed for 48 h with an 8 kDa dialysis bag to produce MnO_2–PEG NPs.

Preparation of hydrogel-3

To prepare the hydrogel, DTBP block polymers were dissolved at 15 wt% in normal saline at 4 °C. Hydrogel-3 was prepared by adding MnO_2–PEG NPs with Mn^{2+} (50 μg mL^{-1}) and GEM to the DTBP solution, followed by heating.

In vitro adhesive strength test of the hydrogel

In accordance with a previous report, fresh pigskin was selected for the evaluation of the adhesion properties of hydrogel-3. The fresh pigskin was cut and immersed in PBS at 30 °C for further processing. Typically, 200 μL of an aqueous hydrogel dispersion was dropped on the surface of a rectangular piece of pigskin (2 × 5 × 0.5 cm^3). Another piece of skin was placed on the hydrogel solution area. Quantitative adhesion properties were measured using the lap shear test on an Instron materials test system (Instron, 5965) equipped with a 50 N load cell at a rate of 5 mm min^{-1}. All measurements were repeated three times.

Injectable properties of hydrogels

The injectable properties of hydrogels were tested on an Instron materials test system (Instron, 5965). The pressure required to pass the hydrogel premix through needles of different sizes was measured, with PBS used as the control.

Drug release *in vitro*

Drug release from the hydrogel was investigated. Briefly, 250 μL of hydrogel containing 500 μg of gemcitabine hydrochloride (GEM) was sealed in a dialysis bag and immersed in 10 mL of the appropriate release medium (PBS solution, pH = 6.5) under a shaker (120 rpm) at 37 °C. At the selected times, 500 μL of the release medium was extracted, followed by the addition of the same volume of fresh buffer. An ultraviolet spectrophotometer (VIS-722 V) was used to measure the concentration of GEM release at 269 nm at each time point. Analysis was performed in triplicate for each condition.

In vitro photothermal performance of hydrogel-3

To elucidate the photothermal effect of hydrogel-3, 1 mL of 15 wt% of the as-prepared hydrogel was placed into a 1.5 mL tube and exposed to an 808 nm near-infrared (NIR) laser at a power density of 1.5 W cm^{-2} for 5 min. The temperature variation was recorded by a photothermal camera (Fluke Ti400).

Cell culture

BxPC-3 cells were purchased from Wuhan Servicebio Technology Co., Ltd and cultured in RPMI-1640 growth medium supplemented with 10% FBS, 50 U per mL penicillin and 50 U per mL streptomycin. Cells were maintained at 37 °C in a humidified 5% CO_2 atmosphere and cultured according to ATCC recommendations.

In vitro cytotoxicity assays and synergy of drug combinations

The relative cytotoxicity of DTBP, GEM, MnO_2–PEG NPs and their combinations (with or without laser) against BxPC-3 human pancreatic adenocarcinoma cell was assessed using an MTT assay. Cells were seeded in 96-well plates at a density of 3500 cells per well in 100 μL culture medium and incubated for 24 h. Then, the medium was replaced with 200 μL of fresh medium containing free GEM (0.1 nM, 1 nM, 2 nM, 5 nM, 10 nM, 15 nM, 20 nM, and 40 nM), free DTBP (15 wt%), free MnO_2–PEG NPs (Mn^{2+} 50 μg mL^{-1}), or a series of combinations of DTBP, GEM and MnO_2–PEG NPs (with or without laser) under the same conditions (n = 6 for each group). After incubation for 48 h at 37 °C, the cells were subjected to an MTT assay, and the absorbance at 570 nm was measured using a microplate reader (Bio-Rad). The relative viability of the treated cells was calculated as the percentage of the untreated control group.

In vivo synergistic thermo-chemotherapy test

Pancreatic cancer xenograft models were established in Balb/c nude mice (male, 20 ± 2 g) purchased from Ziyuan Experimental Animal Technology Co., Ltd. (Hangzhou, China). To establish the pancreatic cancer xenograft models, 6.0 × 10^6 BxPC-3 cells were subcutaneously injected into the right flank regions of the nude mice, followed by a feeding period of two weeks. The tumor-bearing mice were randomly divided into four groups (n = 5 per group) and treated with 100 μL of different formulations *via* intratumoral (i.t.) injection on day 0. The formulations included: hydrogel-1 (with no laser) (i.t.) (group 1), hydrogel-2 (with 808 nm

laser) (i.t.) (group 2), hydrogel-3 (with no laser) (i.t.) (group 3), hydrogel-3 (with 808 nm laser) (i.t.) (group 4). For all drug-containing formulations, the GEM dosage was maintained at 5 mg kg^{-1}. Tumor sizes were measured every two days using a caliper and calculated using the following equation:

$$V = L \times W^2/2,$$

where L and W represent the length and width of the tumor, respectively. The body weight of each mouse was recorded every other day. On day 14 post-treatment, the animals were sacrificed, and the tumors were harvested for H&E staining, Ki-67 staining and TUNEL assay. VX2 xenografted tumor-bearing New Zealand rabbits were used for the study of regional treatment of deep tumors. Briefly, after the rabbits were anesthetized using isoflurane, hydrogel-3 and hydrogel-1 were respectively injected into the VX2 tumor area by laparotomy, followed by hyperthermia treatment for 10 min under an 808 nm laser (1.5 W cm^{-2}). After 1 week, the rabbits were sacrificed, and the tumor tissue was removed for imaging, H&E staining, Ki-67, and TUNEL analyses. All animal experiments were approved by the Animal Care and Use Committee of the University of Science and Technology of China (Hefei, Anhui, 230001, P.R. China) and were carried out in compliance with the approved guidelines (2024-N(A)-008). Images were acquired and processed using a Nikon Ni-U microscope and a Pannoramic Scanner software.

Toxicity evaluation of hydrogel-3

Whole blood from SD rats was used to evaluate the haemolytic potential of the hybrid hydrogels. Briefly, 20 μL of whole blood was added to 5 mL of normal saline containing 5 mg of hydrogel, followed by incubation at 37 °C for 1 h. After centrifugation (2000 rpm, 5 min), the optical densities of the collected supernatants were measured at 545 nm using a UV spectrophotometer. Whole blood incubated with distilled water and normal saline was used as the positive and negative controls, respectively, to investigate the foreign body response of the hybrid hydrogels. Hydrogel-3 was injected subcutaneously into rats for toxicity assessment. Histological analysis (H&E staining) of the major organs (heart, liver, spleen, lung and kidney) was performed to assess potential organ damage 14 days after hydrogel injection. Meanwhile, blood samples were taken for biochemical index evaluation.

Statistical analyses

Mean values, standard deviations and p-values were analyzed using Origin Pro 8.0. All error bars represent the standard deviations. Data were expressed as mean ± S.D. p-Values less than 0.05 were considered statistically significant.

Results

Preparation of hybrid hydrogels

The triblock co-polymers of poly((*N*-isopropylacrylamide-*co*-dopamine)-*b*-poly(ethylene glycol)-*b*-poly(*N*-isopropylacrylamide-*co*-dopamine)) (poly(NIPAM-*co*-DOPA)–PEG–poly(NIPAM-*co*-DOPA)) (denoted as DTBP) were synthesized and employed as the matrix for the hybrid hydrogel preparation. The detailed synthetic process is shown in Fig. S1.† The ^{1}H NMR spectrum of the macro-CTA is shown in Fig. S2a.† The ratio of the integral values between peaks a and b was 55.1/2, which indicated the conjugation of small molecule CTA-NHS on the chain end of the linear PEG precursor. The ^{1}H NMR results of DTBP (Fig. S2c†) suggested the conjugation of dopamine groups onto the polymer chain, and the presence of new peaks at 6.5–6.8 ppm may be attributed to the unoxidized catechol groups.

With good biocompatibility and magnetic response, MnO_2 nanoparticles (NPs) were clinically utilized for the diagnosis and treatment of tumors.[33] Previous studies have demonstrated that MnO_2 NPs with extensive absorption in the near-infrared (NIR) region had photo-responsive ability and good photothermal conversion efficiency to generate spatially and temporally controlled hyperthermia for cancer photothermal therapy (PTT), which was considered a novel PTT photosensitizer.[34,35] PEG–OH was added to a commercially available 100 nm diameter aqueous dispersion of ultrasonically fractured MnO_2 NPs to produce MnO_2–PEG NPs. The zeta potential of these MnO_2 NPs was found to decrease from −22.3 mV for MnO_2–PEG NPs to −20.4 mV after PEGylation, demonstrating the successful coating of PEG onto MnO_2 NPs (Fig. S3d†). The size of the MnO_2–PEG NPs was determined using dynamic light scattering (DLS) to be around 154 nm (Fig. S3c†), which was in agreement with the size observed by transmission electron microscopy (TEM) (Fig. S3b†). In addition, the modified MnO_2–PEG NPs were shown to have good stability in deionised water (Fig. S3a†).

Hydrogels could be prepared from various aqueous suspensions after being immersed in warm water. The hydrogels fabricated from the aqueous suspension of DTBP, the aqueous suspension after being mixed with GEM, and the aqueous suspension after being mixed with GEM and MnO_2–PEG NPs were denoted as hydrogel-1, hydrogel-2 and hydrogel-3, respectively.

In a detailed investigation, as shown in Fig. 1e, a sol–gel transition of the aqueous solution could be observed after immersing in a water bath at 35 °C for hydrogel-3. Rheology measurements were applied to further evaluate this thermal sensitivity (Fig. 1f). The storage and loss modulus (G' and G'') curves of hydrogel-3 during the heating process suggested that the sol–gel transition started from 28 to 29 °C, indicating that the sol–gel transition was sensitive to body temperature. These results suggested the successful preparation of a bio-applicable thermal-responsive hybrid hydrogel. A typical 3D porous structure was observed from the scanning electron microscopy (SEM) images (Fig. 1a) of the freeze-dried hydrogel-3. Energy-dispersive spectroscopy (EDS) elemental mapping images further revealed the homogeneous distribution of MnO_2–PEG NPs in hydrogel-3 (Fig. 1b).

For *in vivo* applications, the mussel-like hydrogel should be capable of adhering to soft tissues under wet conditions to meet the requirement of fixation at targeted sites.[36,37] As shown in Fig. 1g and h, after coupling dopamine groups, the hydrogel exhibited strong adhesion to fresh pig skin (101.33 kPa). The

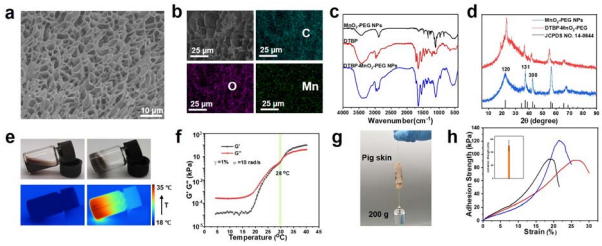

Fig. 1 Characterization of hydrogel-3. (a) SEM image of hydrogel-3. (b) EDS mappings of C, O and Mn elements in hydrogel-3. (c) FT-IR spectra of MnO_2–PEG NPs and DTBP. (d) XRD pattern of MnO_2–PEG NPs and DTBP–MnO_2–PEG NPs. (e) Digital images and infrared thermal images of DTBP–GEM–MnO_2–PEG NPs aqueous dispersion (hydrogel-3) during the heating process. (f) G'/G'' measurements of the DTBP–GEM–MnO_2–PEG NPs aqueous dispersion (hydrogel-3). (g) Digital images and (h) corresponding adhesion strength of hydrogel-3 adhered to pig skin.

adhesion properties in this humid environment were similar to previous reports.[34,38,39] The matrix DTBP of hydrogel-3 contains dopamine (DOPA). Upon oxidation, the catechol group in dopamine can undergo oxidation. Tissue surfaces, such as skin and mucous membranes, possess amino or sulfhydryl groups. The oxidized catechol group can covalently bond with these functional groups, thereby firmly attaching the hydrogel to the tissue (Fig. S4†). This covalent bonding ensures that the hydrogel adheres securely to the tissue surface, reducing the likelihood of detachment and enhancing both its fixation and therapeutic efficacy *in vivo*.[40–42] Additional demonstration using rat-isolated pancreatic tissue in 37 °C PBS (simulating the *in vivo* abdominal environment) also suggested the strong adhesion property. As such, hydrogel-3 could qualify for continuous fixation at the tumor site for therapeutic action. The injectability of hydrogel-3 aqueous suspensions through different needles was measured with a mechanical tester (Fig. S5†). The results showed that hydrogel-3 exhibited good injectability through different types of needles, which encouraged its invasive administration.

Drug release, photothermal property, and *in vitro* experiments of hydrogel-3

The release and diffusion of drugs from hydrogels into tumor tissue after intratumoral injection are vital for the effective treatment of PC.[43,44] The collapse of the hydrogel network would facilitate drug release. In our experiments, the GEM diffusion behavior of hydrogel-3 was investigated using agar gel phantom tumor tissues. To simulate the internal acidic microenvironment, a model tissue with a pH of 6.5 was applied. Results suggested that the drug diffused from the interior of the composite hydrogel to exert a therapeutic effect continuously within 14 days, and the diffusion rate reached 52% at 14 days (Fig. S6†). These results indicated that GEM could be effectively released from the hydrogel in an acidic microenvironment.

The time-dependent temperature profiles and infrared thermograms of hydrogel-3 under 808 nm laser irradiation are shown in Fig. 2a and b, respectively, demonstrating the excellent photothermal properties. In the *in vitro* experiments, after being exposed to the 808 nm laser irradiation, the temperature of the composite hydrogel approached 50.9 °C from 11.4 °C (ΔT = 39.5 °C) within 5 min. However, no temperature increase was observed in the hydrogel-1 dispersion. These results suggested that the incorporation of MnO_2–PEG NPs contributed to the effective photothermal heating of the composite hydrogel, which could be applied to kill pancreatic cancer cells with negligible side effects on normal cells.

The combination of chemotherapy and photothermal therapy (PTT) has received considerable research attention recently due to its high selectivity and excellent therapeutic effects.[45–49] PTT increases the local temperature of the tumor tissue, accelerates the denaturation of tumor cell proteins and the rate of chemical reactions between drugs and DNA, and inhibits the activity of tumor cell DNA repair enzymes, thus facilitating the synthesis and repair of DNA by chemotherapy.[50,51] In a synergistic chemotherapeutic strategy, the heat generated by PTT can also enhance the therapeutic effect by improving the permeability of cell membranes, accelerating drug uptake at the tumor site, and promoting drug retention in tumor tissues through the enhanced permeability and retention (EPR) effect.[46,52,53]

Therefore, we investigated the effects of a range of material combinations and the presence or absence of laser light on the survival of BxPC-3 cells using the MTT method (Fig. S7a and b†). After incubation for 48 h, DTBP–GEM combined treatment showed a dose-dependent anti-proliferative activity, and DTBP did not affect the production of chemotherapy. Under the same conditions, a series of experimental results showed that the laser combined with DTBP–GEM–MnO_2–PEG NPs had the best synergistic inhibitory effect on cell proliferation.

In vivo therapy of subcutaneous tumors in mice

The BxPC-3 tumor-bearing nude mice were employed to evaluate the anti-tumor effect of the hydrogels in the presence of 808 nm

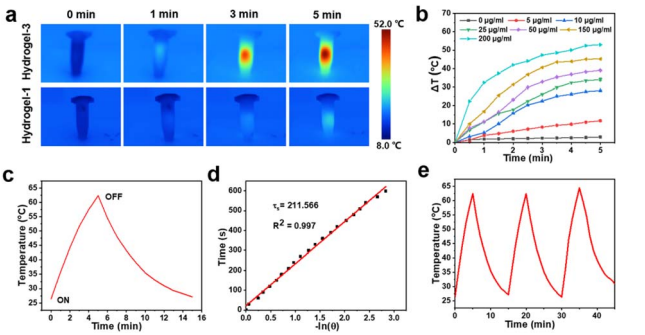

Fig. 2 (a) Infrared thermal images of hydrogel-1 and hydrogel-3 under 808 nm laser irradiation *in vitro*. (b) Temperature rise efficacy with various concentrations of Mn^{2+} in hydrogel-3 *in vitro*. (c) Photothermal performance of the aqueous dispersion of hydrogel-3 under NIR irradiation by 808 nm laser at a power intensity of 1.5 W cm^{-2} for specified periods, with the laser cut off when the temperature tended to stabilize. (d) Time constant for heat transfer calculated from the cooling period. (e) Heating curve of hydrogel-3 dispersed in water for three cycles at a power intensity of 1.5 W cm^{-2} under irradiation by a 808 nm laser.

laser irradiation. The hyperthermia process at the tumor site was monitored *in situ* with an infrared thermometer. The temperature of the tumor site in hydrogel-3 with the 808 nm laser was raised to approximately 50 °C within 5 min (Fig. 3a and b). This hyperthermia effect was appropriate to induce tumor coagulation necrosis, as reported previously.[54–56] In comparison with the tumors showing continuous progression in other groups, it was found that the tumor in the hydrogel-3 + 808 nm laser group was significantly reduced or even disappeared after 14 days of treatment (Fig. 3c and e). Moreover, the H&E and TUNEL analyses of tumor sections showed the largest area of markedly apoptotic cells in the hydrogel-3 + 808 nm laser group (Fig. 4a). However, no significant cell apoptosis occurred in the other treatment groups. Previous studies have demonstrated that higher Ki-67 levels are associated with a higher risk of tumor spread and recurrence, as well as faster tumor growth.[57–63] In PC, the overexpression of Ki-67 is a driver of tumor cell metastasis and has a negative effect on the chemotherapy response.[64,65] Compared with the hydrogel-1 group, the expression of Ki-67 in the hydrogel-3 + 808 nm laser group was considerably lower than those in the control group, and the cellular signal of apoptosis was significantly enhanced. These results suggest that hydrogel-3 may be feasible as a novel therapeutic approach for the combination of local chemotherapy and photothermal therapy in the treatment of PC.

In situ treatment of hydrogel-3 in rabbit PC

The pathobiological features of PC are complex, so it is crucial to establish an *in situ* pancreatic cancer model. The orthotopic pancreatic cancer-bearing rabbits were established to investigate the anti-tumor effect of the hydrogel-3 + 808 nm laser group. The specific location of orthotopic PC was confirmed by computed tomography (CT) (Fig. 5b). As shown in Fig. 5c, the prepared solution was injected into the PC through laparotomy surgery. The temperature of tumor sites in the hydrogel-3 (with 808 nm laser) group increased from 36 to 56 °C within 10 min (Fig. 5a and d). This hyperthermia was sufficient to inhibit tumor growth, as reported in previous studies.[66] On the 7th day after treatment, the rabbits were sacrificed, and the tumor tissues were dissected for H&E staining, Ki-67, and TUNEL analyses, respectively. Visible necrosis of the tumor tissues appeared around the hydrogel-3 (with 808 nm laser) injection site. Compared with other groups,

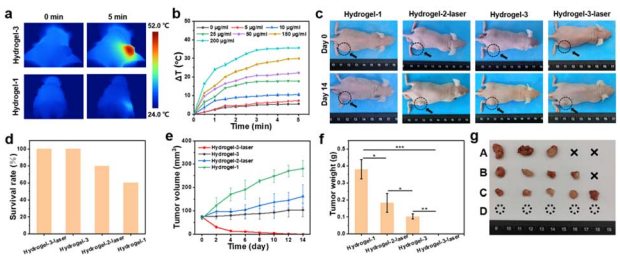

Fig. 3 *In vivo* combination treatment of BxPC-3 tumor in the nude mice model. (a) Infrared thermal images of hydrogel-1 and hydrogel-3. (b) Temperature changes in mice corresponding to various concentrations of Mn^{2+} in hydrogel-3 after exposure to a 808 nm laser. (c) Photographs of postoperative mice from various treatment groups on days 0 and 14. Arrows on day 0 indicate the baseline tumor status prior to administration, and arrows on day 14 indicate whether the tumor grew or disappeared. (d) Survival rate and (e) tumor volume of different groups over 14 days. (f) Tumor weight in different groups at the 14 day time point and (g) digital images of tumor tissues obtained from various groups at the 14 day time point. Hydrogel-1 (no laser) (group A), hydrogel-2 (with 808 nm laser) (group B), hydrogel-3 (no laser) (group C), hydrogel-3 (with 808 nm laser) (group D). Some of the mice in groups A and B died before the end of the experiment and are indicated with an × symbol. All tumor volumes in group D were below the minimum detectable volume (5 mm^3) and are indicated by dashed circles. Data are presented as the mean ± S.D. ($n = 5$). *$p < 0.05$; **$p < 0.01$; ***$p < 0.001$.

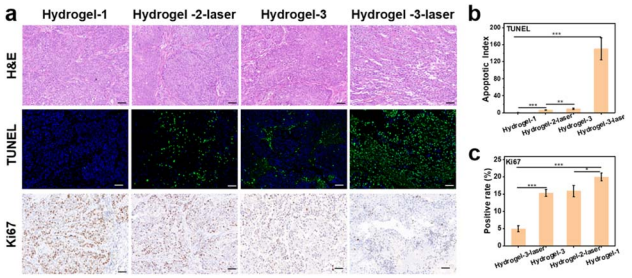

Fig. 4 *Ex vivo* histological analysis of tumor sections after H&E staining, Ki-67 staining and TUNEL assay (14 days after treatment). (a) Representative microphotographs of tumor slices. (b) Percentage of apoptotic cells in tumors after treatment. (c) The corresponding positive ratio of Ki-67 staining. Data are expressed as mean ± S.D. ($n = 3$). *$p < 0.05$, **$p < 0.01$ and ***$p < 0.001$ by Student's *t*-test. Scale bar: 50 μm.

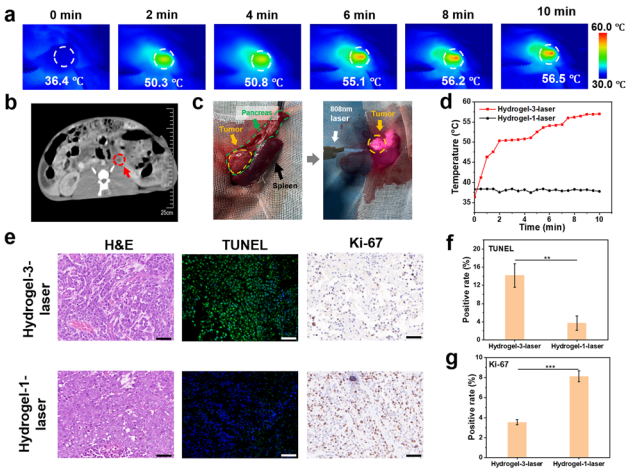

Fig. 5 The orthotopic pancreatic cancer-bearing rabbits were established to evaluate the ability of hydrogel-3 (with a 808 nm laser) to suppress the tumor. (a) Infrared thermal images and (d) corresponding temperature change of postoperative tumor sites treated with hydrogel-3 under a 808 nm laser (1.5 W cm^{-2}). (b) The PC in rabbits was confirmed with CT in coronal plane scan. The red dotted line region indicates the PC. (c) The images of the PC through laparotomy surgery and after receiving laser treatment following the injection of the DTBP–GEM–MnO_2–PEG NPs solution into the tumor. *Ex vivo* histological analysis of tumor sections after H&E staining, Ki67, and TUNEL analyses (seven days after treatment). (e) Representative microphotographs of tumors slices. (f) Percentage of apoptotic cells in tumors after treatment. (g) The corresponding positive ratio of Ki-67 staining. Data are expressed as mean ± S.D. ($n = 3$). *$p < 0.05$, **$p < 0.01$ and ***$p < 0.001$ by Student's *t*-test. Scale bar: 50 μm.

the related results (H&E staining, Ki-67, and TUNEL images in the tumor sections) from the hydrogel-3 (with 808 nm laser) group exhibited remarkable absence of nuclei, significant necrosis, and enhanced apoptosis induction of residual tumor cells (Fig. 5e–g).

Overall, the above results strongly suggested that the treatment combined with chemotherapy and 808 nm laser irradiation after *in situ* implantation of hydrogel-3 was a promising therapeutic approach for PC. Compared to previous studies on traditional treatment and multidisciplinary treatment of PC, such as chemotherapy,[67] immunotherapy,[68] and photothermal combined with immunotherapy,[69] we developed an *in situ* injectable hydrogel platform combined with photothermal and chemotherapy, which can help completely eliminate *in situ* PC tumors in a short time.

Biocompatibility evaluation

The cytotoxicity assays of human umbilical vein endothelial cells (HUVECs) were investigated to evaluate the cytocompatibility of the hydrogels. No cytotoxicity to HUVECs was observed after incubation with the free DTBP and free MnO_2-PEG NPs, respectively (Fig. S8†). As shown in Fig. S9,† the main indicators of kidney and liver function remained within the normal range 14 days after implantation of hydrogel-3. In the H&E staining images, there were no significant histopathological abnormalities or lesions in the vital organs (heart, liver, spleen, lung, and kidney) (Fig. S9†), and the major serum and key hematological indices remained within normal limits (Fig. S10†). In addition, no hemolysis of whole blood was induced by the hybrid hydrogels (Fig. S11†). These results indicated that the composite hydrogel exhibited good biocompatibility.

Conclusions

In summary, we presented a thermo-responsive hydrogel as a new agent for PC treatment. The highly injectable hydrogel-3 exhibited drug release behavior and efficient thermogenesis under 808 nm laser irradiation. The hydrogel-3 + 808 nm laser group successfully achieved the synergistic treatment of photothermal therapy and local chemotherapy for unresectable PC, which will impact the clinical applications of hydrogels, in addition to the comprehensive treatment strategy for pancreatic cancer and other solid tumors.

Data availability

The authors confirm that the data supporting the findings of this study are available within the article or in its ESI.†

Conflicts of interest

There are no conflicts to declare.

Acknowledgements

This work was financially supported by the National Natural Science Foundation of China (No. 52302347), the National Natural Science Foundation of China (22171067), the "Research Funds of Center for Leading Medicine and Advanced Technologies of IHM" (2023IHM01090, 2023IHM01093), the Joint Fund for Medical Artificial Intelligence (MAI2023C007), the National Natural Science Foundation of China (31870993), and the Fundamental Research Funds for the Central Universities (WK9110000005).

Notes and references

1 H. M. Kolbeinsson, S. Chandana, G. P. Wright and M. Chung, *J. Invest. Surg.*, 2023, **36**, 2129884.
2 X. Chen, H. J. Zeh, R. Kang, G. Kroemer and D. Tang, *Nat. Rev. Gastroenterol. Hepatol.*, 2021, **18**, 804–823.
3 L. D. Wood, M. I. Canto, E. M. Jaffee and D. M. Simeone, *Gastroenterology*, 2022, **163**, 386–402.
4 R. L. Siegel, K. D. Miller and A. Jemal, *Ca-Cancer J. Clin.*, 2020, **70**, 7–30.
5 U. Hayat, P. S. Croce, A. Saadeh, K. Desai, J. Appiah, S. Khan, Y. I. Khan, K. Kumar and A. Hanif, *J. Clin. Med.*, 2025, **14**(4), 1129.
6 T. Gupta and M. Murtaza, *Prog. Biophys. Biophys. Chem.*, 2025, **196**, 19–32.
7 P. P. Adiseshaiah, R. M. Crist, S. S. Hook and S. E. McNeil, *Nat. Rev. Clin. Oncol.*, 2016, **13**, 750–765.
8 A. A. Rucki and L. Zheng, *World J. Gastroenterol.*, 2014, **20**, 2237–2246.
9 D. von Ahrens, T. D. Bhagat, D. Nagrath, A. Maitra and A. Verma, *J. Hematol. Oncol.*, 2017, **10**, 76.
10 S. Jiang, J. B. Fagman, Y. Ma, J. Liu, C. Vihav, C. Engstrom, B. Liu and C. Chen, *Aging*, 2022, **14**, 7635–7649.
11 J. Li, M. G. Wientjes and J. L. Au, *AAPS J.*, 2010, **12**, 223–232.
12 V. Tonini and M. Zanni, *World J. Gastroenterol.*, 2021, **27**, 5851–5889.
13 A. L. Lucas and F. Kastrinos, *JAMA*, 2019, **322**, 407–408.
14 Y. Fu, L. Chen, N. Lv, J. Wang, S. Yu, Q. Fang and W. Xin, *Mol. Carcinog.*, 2025, DOI: **10.1002/mc.23914**.
15 Q. Hu, C. Jiang, Y. Qin, B. Li, J. Wang, T. Wang, S. Ji, Z. Ye, Q. Dang, M. Liu, X. Yu and X. Xu, *Cancer Lett.*, 2025, **618**, 217633.
16 Z. Zhang, Y. Wang, S. Xu, Y. Yu, A. Hussain, Y. Shen and S. Guo, *J. Mater. Chem. B*, 2017, **5**, 5464–5472.
17 H.-J. Cai, T.-T. Shen, J. Zhang, C.-F. Shan, J.-G. Jia, X. Li, W.-S. Liu and Y. Tang, *J. Mater. Chem. B*, 2017, **5**, 2390–2394.
18 N. Iosifidou, E. Anagnostopoulou, M. Botou, E. Kalfa, E. Tatsaki and S. Frillingos, *Int. J. Mol. Sci.*, 2024, **25**(13), 7012.
19 J. Hong, S. Xian, S. Zheng, *et al.*, *Nano Res.*, 2024, **17**, 8377–8388.
20 Q. Hu, F. Zhang, B. Li, P. Jin, J. Huang, Z. Yao, X. Zhao, S. Shao, M. Wang, Y. Ping and T. Liang, *Small*, 2025, 2410629.
21 M. Amrutkar and I. P. Gladhaug, *Cancers*, 2017, **9**(11), 157.
22 Y. Zhang, H. C. Crawford and M. P. di Magliano, *Annu. Rev. Physiol.*, 2019, **81**, 211–233.
23 T. Kamisawa, L. D. Wood, T. Itoi and K. Takaori, *Lancet*, 2016, **388**, 73–85.
24 L. Wang, M. Neumann, T. Fu, W. Li, X. Cheng and B.-L. Su, *Curr. Opin. Colloid Interface Sci.*, 2018, **38**, 135–157.

25 P. Lavrador, M. R. Esteves, V. M. Gaspar and J. F. Mano, *Adv. Funct. Mater.*, 2020, **31**(8), DOI: 10.1002/adfm.202005941.
26 P. Rahmanian-Devin, V. B. Rahimi and V. R. Askari, *Adv. Pharmacol. Pharm. Sci.*, 2021, **2021**, 6640893.
27 R. Narayanaswamy and V. P. Torchilin, *Molecules*, 2019, **24**(3), 603.
28 B. Farasati Far, M. R. Naimi-Jamal, M. Safaei, K. Zarei, M. Moradi and H. Y. Nezhad, *Polymers*, 2022, **14**(24), 5432.
29 S. Sang, Z. Jiang, N. Xie, H. Rao, K. Liao, Q. Hu, Z. Zhang, R. Guo, T. Fan and K. Deng, *Nanophotonics*, 2021, **10**, 2625–2637.
30 X. Li, Y. Hou, X. Meng, C. Ge, H. Ma, J. Li and J. Fang, *Angew. Chem., Int. Ed. Engl.*, 2018, **57**, 6141–6145.
31 X. Yan, T. Sun, Y. Song, W. Peng, Y. Xu, G. Luo, M. Li, S. Chen, W.-W. Fang, L. Dong, S. Xuan, T. He, B. Cao and Y. Lu, *Nano Lett.*, 2022, **22**, 2251–2260.
32 L. Ning, C. You, Y. Zhang, X. Li and F. Wang, *Life Sci.*, 2020, **241**, 117137.
33 G. Yang, J. Ji and Z. Liu, *Wiley Interdiscip. Rev.:Nanomed. Nanobiotechnol.*, 2021, **13**, e1720.
34 Z. Xiao, Q. Li, H. Liu, Q. Zhao, Y. Niu and D. Zhao, *Eur. Polym. J.*, 2022, **173**, 111277.
35 Z. Liu, S. Zhang, H. Lin, M. Zhao, H. Yao, L. Zhang, W. Peng and Y. Chen, *Biomaterials*, 2018, **155**, 54–63.
36 L. Han, X. Lu, K. Liu, K. Wang, L. Fang, L.-T. Weng, H. Zhang, Y. Tang, F. Ren, C. Zhao, G. Sun, R. Liang and Z. Li, *ACS Nano*, 2017, **11**, 2561–2574.
37 W. Zhang, R. Wang, Z. Sun, X. Zhu, Q. Zhao, T. Zhang, A. Cholewinski, F. Yang, B. Zhao, R. Pinnaratip, P. K. Forooshani and B. P. Lee, *Chem. Soc. Rev.*, 2020, **49**, 433–464.
38 K. Zhang, Q. Feng, Z. Fang, L. Gu and L. Bian, *Chem. Rev.*, 2021, **121**, 11149–11193.
39 X. Xu, X. Xia, K. Zhang, A. Rai, Z. Li, P. Zhao, K. Wei, L. Zou, B. Yang, W.-K. Wong, P. W.-Y. Chiu and L. Bian, *Sci. Transl. Med.*, 2020, **12**, eaba8014.
40 Y. Liu, H. Meng, P. B. Messersmith, B. P. Lee and J. L. Dalsin, in *Biological Adhesives*, ed. A. M. Smith, Springer International Publishing, Cham, 2016, pp. 345–378, DOI: 10.1007/978-3-319-46082-6_15.
41 L. Wang and J. Liu, *Acc. Chem. Res.*, 2024, **57**(6), 945–956.
42 W. Dou, X. Zeng, S. Zhu, Y. Zhu, H. Liu and S. Li, *Int. J. Mol. Sci.*, 2024, **25**, 9100.
43 Y. Zheng, Y. Cheng, J. Chen, J. Ding, M. Li, C. Li, J. C. Wang and X. Chen, *ACS Appl. Mater. Interfaces*, 2017, **9**, 3487–3496.
44 R. Fan, A. Tong, X. Li, X. Gao, L. Mei, L. Zhou, X. Zhang, C. You and G. Guo, *Int. J. Nanomed.*, 2015, **10**, 7291–7305.
45 J. Wang, J. Chai, L. Liu, Z. Cui, D. Duan, R. Shi and Y. Zhang, *RSC Adv.*, 2019, **9**, 3012–3019.
46 H.-X. Tang, C.-G. Liu, J.-T. Zhang, X. Zheng, D.-Y. Yang, R. K. Kankala, S.-B. Wang and A.-Z. Chen, *ACS Appl. Mater. Interfaces*, 2020, **12**, 47289–47298.
47 R. Chen, F. Yang, Y. Xue, X. Wei, L. Song and X. Liu, *RSC Adv.*, 2016, **6**, 38931–38942.
48 X. Li, Y. Wang, T. Liu, Y. Zhang, C. Wang and B. Xie, *Colloids Surf., B*, 2023, **225**, 113288.
49 X. Li, M. Yang, J. Cao, H. Gu, W. Liu, T. Xia, W. Sun, J. Fan and X. Peng, *ACS Mater. Lett.*, 2022, **4**, 724–732.
50 Y. Liu, X. Zhang, L. Luo, L. Li, R. Y. Zhu, A. Li, Y. He, W. Cao, K. Niu, H. Liu, J. Yang and D. Gao, *Nanomedicine*, 2019, **18**, 303–314.
51 A. Li, S. Wang, Z. Zhang, N. Xu, G. Ling and P. Zhang, *J. Mater. Chem. B*, 2022, **10**, 5191–5202.
52 X. M. Zhu, H. Y. Wan, H. Jia, L. Liu and J. Wang, *Adv. Healthcare Mater.*, 2016, **5**, 3165–3172.
53 S. Yang, P. Yang, Y. Xie, B. Zhang, J. Lin, J. Fan and Z. Zhao, *J. Mater. Sci.*, 2021, **56**, 18219–18232.
54 S. Zhu, S. Wang, C. Liu, M. Lyu and Q. Huang, *Front. Oncol.*, 2022, **12**, 918416.
55 C. Gu, J. Zhang, W. Gao, J. Wang, K. Mou, X. Zhang and J. Qi, International Communications in Heat and Mass Transfer, 2025, 164:, *Int. Commun. Heat Mass Transfer*, 2025, **164**, 108895.
56 K.-Y. Qian, Y. Song, X. Yan, L. Dong, J. Xue, Y. Xu, B. Wang, B. Cao, Q. Hou, W. Peng, J. Hu, K. Jiang, S. Chen, H. Wang and Y. Lu, *Biomaterials*, 2020, **259**, 120299.
57 A. Akbarnejad, N. Ray, P. J. Barnes and G. Bigras, *Appl. Immunohistochem. Mol. Morphol.*, 2025, DOI: 10.1097/PAI.0000000000001258.
58 T. Li, X.-H. Yang, M.-J. Shao, Y.-X. Dong, L.-Y. Li and C.-Z. Lin, *Sci. Rep.*, 2025, 10062.
59 M. Pellicciaro, M. Materazzo, A. Bertolo, F. Tacconi, S. A. Bastone, F. Calicchia, D. Eskiu, E. Toscano, A. Sadri, M. Treglia, M. Berretta, B. Longo, V. Cervelli, O. C. Buonomo and G. Vanni, *Cancers*, 2025, **17**, 798.
60 L. T. Senbanjo and M. A. Chellaiah, *Front. Cell Dev. Biol.*, 2017, **5**, 18.
61 A. Gupta, C. Q. Zhou and M. A. Chellaiah, *Cancers*, 2013, **5**, 617–638.
62 M. Todaro, M. Gaggianesi, V. Catalano, A. Benfante, F. Iovino, M. Biffoni, T. Apuzzo, I. Sperduti, S. Volpe, G. Cocorullo, G. Gulotta, F. Dieli, R. De Maria and G. Stassi, *Cell Stem Cell*, 2014, **14**, 342–356.
63 J. Gu, Y. Guo, J. Du, L. Kong, J. Deng, B. Tao, H. Li, C. Jin, D. Fu and J. Li, *Cancers*, 2022, **14**, 5434.
64 S. Zhao, C. Chen, K. Chang, A. Karnad, J. Jagirdar, A. P. Kumar and J. W. Freeman, *Clin. Cancer Res.*, 2016, **22**, 5592–5604.
65 W. Mu, Y. Xu, P. Gu, W. Wang, J. Li, Y. Ge and H. Wang, *Engineering*, 2021, **7**, 1413–1423.
66 W.-S. Wu, X. Yan, S. Chen, Y. Du, J. Hu, Y. Song, Z. Zha, Y.-J. Xu, B. Cao, S.-H. Xuan, X. Liu, B. Chen, L. Dong, Y. Lu and S.-H. Yu, *Adv. Mater.*, 2024, **36**, 2309770.
67 J. Wang, J. Yang, A. Narang, *et al.*, *J. Hematol. Oncol.*, 2024, **17**, 92.
68 X. Ge, K. Zhang, J. Zhu, Y. Chen, Z. Wang, P. Wang, P. Xu and J. Yao, *Int. J. Biol. Sci.*, 2025, **21**(1), 63–74.
69 Y. Hu, E. Qi, C. Yun, X. Li, F. Liu, Z. Cheng, N. Guan, Q. Wang, H. Zhao, W. Xiao, L. Peng, J. Yang and X. Yu, *J. Transl. Med.*, 2025, **23**, 271.